Eur. Phys. J. B **14**, 733–746 (2000)

THE EUROPEAN PHYSICAL JOURNAL B

EDP Sciences

Comparison of density-functional approaches and Monte Carlo simulations for free planar films of liquid ^{4}He

L. Szybisz[a]

Laboratorio TANDAR, Departamento de Física, Comisión Nacional de Energía Atómica, Av. del Libertador 8250, RA-1429 Buenos Aires, Argentina
and
Departamento de Física, Facultad de Ciencias Exactas y Naturales, Universidad de Buenos Aires, Ciudad Universitaria, RA-1428 Buenos Aires, Argentina

Received 26 July 1999

Abstract. Density functionals proposed in the literature for describing the behaviour of liquid helium at $T = 0$ K are examined. In so doing, several properties of the ground states of free films of superfluid ^{4}He are calculated by using zero- and finite-range density functional theories and these results are compared to that computed with Monte Carlo simulations. We mainly focus the attention on the energy per particle of the slabs, the surface tension and the width of the liquid-vacuum interfaces, all as a function of the inverse of coverage. The largest differences are found in the case of the surface widths.

PACS. 61.20.-p Structure of liquids – 67.70.+n Films (including physical adsorption) – 68.10.-m Fluid surfaces and fluid-fluid interfaces

1 Introduction

During the last decade a great progress has been achieved in understanding properties of inhomogeneous systems of liquid ^{4}He. A survey of examples of experimental and theoretical developments may be found, for instance, in the proceedings of international symposia on quantum fluids and solids published in [1–3].

As well-known, the ground-state energy of an interacting N-body system of ^{4}He atoms, immersed in an external potential due to a substrate $U_{\rm sub}(\mathbf{r})$, may be written as

$$E_{\rm gs} = -\frac{\hbar^2}{2m}\int {\rm d}\mathbf{r}\,\sqrt{\rho(\mathbf{r})}\nabla^2\sqrt{\rho(\mathbf{r})} + \int {\rm d}\mathbf{r}\,\rho(\mathbf{r})\,e_{\rm c}(\mathbf{r}) + \int {\rm d}\mathbf{r}\,\rho(\mathbf{r})\,U_{\rm sub}(\mathbf{r}), \quad (1.1)$$

where $\rho(\mathbf{r})$ is the one-body density. The first term on the right-hand side is the quantum kinetic energy of the helium particles of mass m. The second term represents the interaction between the particles of the system, where $e_{\rm c}(\mathbf{r})$ is the correlation energy per particle depending on the approach adopted for the theoretical description. We shall come back to this point later on. The last term is the interaction with the external field.

The spatial particle distribution $\rho(\mathbf{r})$ in the ground state is determined by minimizing the total energy of the system with respect to the density. This is usually accomplished by applying a variational procedure with the constraint of a fixed particle number N, *i.e.*,

$$\frac{\delta[E_{\rm gs} - \mu N]}{\delta\sqrt{\rho(\mathbf{r})}} = 0. \quad (1.2)$$

Here μ is the chemical potential and N is defined as

$$N = \int {\rm d}\mathbf{r}\,\rho(\mathbf{r}). \quad (1.3)$$

The variation of (1.2) leads to a Hartree like equation for the square root of the one-body density

$$\left[-\frac{\hbar^2}{2m}\nabla^2 + V_{\rm H}(\mathbf{r}) + U_{\rm sub}(\mathbf{r})\right]\sqrt{\rho(\mathbf{r})} = \mu\sqrt{\rho(\mathbf{r})}, \quad (1.4)$$

which also determines μ. Here $V_{\rm H}(\mathbf{r})$ is a Hartree mean-field potential given by the first functional derivative of the total correlation energy $E_{\rm c}[\rho]$

$$V_{\rm H}(\mathbf{r}) = \frac{\delta E_{\rm c}[\rho]}{\delta\rho(\mathbf{r})} = \frac{\delta}{\delta\rho(\mathbf{r})}\int {\rm d}\mathbf{r}'\,\rho(\mathbf{r}')\,e_{\rm c}(\mathbf{r}'). \quad (1.5)$$

There are mainly two different self-consistent microscopic approaches to treat the correlation energy [4]. One is an *ab initio* variational method based on the correlated basis theory in conjunction with a perturbative treatment

[a] Also at the Carrera del Investigador Científico of the Consejo Nacional de Investigaciones Científicas y Técnicas, Av. Rivadavia 1917, RA–1033 Buenos Aires, Argentina.
e-mail: szybisz@tandar.cnea.gov.ar

of the hypernetted chain expansion (CBF-HNC) [5–9]. In this procedure one starts from a bare two-body helium-helium interaction (described either by a standard Lennard-Jones (LJ) potential or by a more elaborated one like that of Aziz *et al.* [10]) and solves self-consistently a couple of Euler-Lagrange equations in order to obtain all the quantities of interest. This theory has a "built in" consistency test in the sense that the equations cease to have solutions if the assumed geometry of the system under consideration is unstable against infinitesimal density fluctuations [5,7]. A widely used alternative procedure is of semi-phenomenological nature, where one assumes a density functional (DF) for the correlation energy per particle in terms of $\rho(\mathbf{r})$ and determines the introduced free parameters by fitting properties of bulk ^{4}He system [4]. In this case the ground-state configuration is also evaluated self-consistently. Since the latter theories rely on phenomenological inputs from uniform systems, the validity of the extrapolation to inhomogeneous liquid must always be carefully controlled. Moreover, this approach has not any "built in" consistency test, the stability of the systems must be examined by applying a criterion devised *ad hoc*. On the other hand, the DF calculations are computationally simpler than the CBF-HNC ones. It is important to remark that, DF studies have predicted fascinating phenomena like non-wetting of heavy-alkali metals by liquid ^{4}He at zero absolute temperature [11].

A completely different *ab initio* procedure is based on Monte Carlo (MC) techniques. Because of the relative simplicity of the helium-helium interaction, helium systems can be accurately solved by MC algorithms. The results provided by simulations are usually accepted as exact and can be used to test calculations performed with other theories.

The aim of the present work is to check the accuracy of DF theories by examining their predictions beyond the bulk liquid. For this purpose, we shall compare the outputs of such approaches for inhomogeneous ^{4}He systems with results obtained from MC methods. In particular, we shall focus our attention on free films with planar geometry, for which Vallés and Schmidt [12] have carried out detailed calculations. The films of this kind are invariant in the x-y plane and present a structure along the z coordinate. In fact, it has been demonstrated in [13,14] that free slabs of ^{4}He at $T = 0$ K are unstable and therefore do not exist isolated in nature. However, these systems with densities smaller than the equilibrium bulk density (see Figs. 1 and 2 of [12]) may be associated with substructures as growing layers of adsorbed films (see for example Fig. 8 of [9]). Therefore, it becomes important to test the results provided by the DF theory for free films.

Monte Carlo simulations converge even though the analyzed films are unstable. This is due to the fact that in these procedures periodic boundary conditions are imposed on the x-y plane [12,15] which automatically stabilize the calculated systems because the longest wavelength is the size of the box. Since the instability of the systems is in the limit of very-long wavelengths [13], it cannot be detected by these MC algorithms. As in the case of DF approaches the test for stability should be done separately. So that MC computations provide suitable results for our purpose.

Several different proposals for the correlation energy formulated in the DF theory are summarized in Section 2. The treatment of the energetics for planar ^{4}He systems is provided in Section 3.2. Section 4 is devoted to report numerical results and their analysis and discussion. The final remarks are given in Section 5.

2 Density functionals

A well-known theorem due to Hohenberg and Kohn [16] insures that the energy of a many-body system of interacting particles can be written as a functional of the one-body density. However, it does not provide a practical way of constructing the functional. The main objective of theoretical considerations is a description of this functional. Since the pioneering work of Saam and Ebner [17] several successive proposals have been done for the structure of a reasonable expression for the correlation energy. We shall now outline the characteristics of extensively used DF formalisms, and in a next section present the results obtained for free slabs of ^{4}He.

2.1 Skyrme-type density functional

The simplest DF successfully employed to interpret properties of ^{4}He systems has been proposed by Stringari and Treiner [18]. It is a zero-range correlation inspired in functionals derived by using a phenomenological interaction of Skyrme type [19], which have been extensively applied to describe properties of atomic nuclei. The explicit form assumed in [18] for the correlation energy per particle is

$$e_{\mathrm{c}}^{\mathrm{Sky}}(\mathbf{r}) = \frac{b_4}{2}\,\rho(\mathbf{r}) + \frac{c_4}{2}\,\rho^{\gamma_4+1}(\mathbf{r}) + d_4\,\frac{\mid \nabla\rho(\mathbf{r}) \mid^2}{\rho(\mathbf{r})}\cdot \quad (2.1)$$

Here, the term proportional to b_4 corresponds to an attractive two-body contact force which reflects the attractive character of the interatomic potential at large distances. The term in c_4 is a repulsive, density-dependent contact interaction which dominates at high densities. Finally the term proportional to d_4 reflects the repulsive interaction at the surface. The phenomenological parameters b_4, c_4, and γ_4 have been fixed so as to reproduce known saturation properties of the bulk liquid; while d_4 is adjusted to the surface tension.

For a uniform liquid of density ρ the energy per particle, e_{u}, arising from functional (2.1) takes the form

$$e_{\mathrm{u}} = \frac{E}{N} = \frac{b_4}{2}\,\rho + \frac{c_4}{2}\,\rho^{\gamma_4+1}. \quad (2.2)$$

Pressure and compressibility can be derived directly by taking the first and second derivative of the energy

$$P = \rho^2\,\frac{\partial}{\partial\rho}\left(\frac{E}{N}\right) = \frac{b_4}{2}\,\rho^2 + \frac{\gamma_4+1}{2}\,c_4\,\rho^{\gamma_4+2}, \quad (2.3)$$

$$\frac{1}{\rho\kappa_v} = \frac{\partial P}{\partial\rho} = b_4\,\rho + \frac{(\gamma_4+1)(\gamma_4+2)}{2}\,c_4\,\rho^{\gamma_4+1}. \quad (2.4)$$

Table 1. Parameters of the density functionals for the correlation energy per particle e_c.

Functional	b_4 [K]	γ_4	c_4 [$\times 10^7$ K Å$^{3(\gamma_4+1)}$]	d_4 [$\times 10^3$ K Å^5]	h_{OP} [Å]	b_{LJ} [Å]			Ref.
Skyrme-DF	−888.810	2.8	1.045 54	2.383					[18]
OP-NLDF	−888.810	2.8	1.045 54		2.376 728				[24]
C-NLDF	−888.810	2.8	1.045 54		2.376 728	20.00			[28]
	b'_4 [K]	c'_4 [$\times 10^4$ K Å^6]	c''_4 [$\times 10^6$ K Å^9]		h_{OT} [Å]	α_s [Å^3]	ρ_{0s} [Å^{-3}]	ℓ [Å]	
OT-NLDF	−718.990	−2.411 857	1.858 496		2.190 323	54.31	0.04	1	[31]

At equilibrium (where $P = 0$) the saturation observables, *i.e.*, the equilibrium density, the minimum energy per particle, and the compressibility quoted in Table II of [18] are correctly reproduced with the set of parameters b_4, c_4, and γ_4 listed in Table 1. In order to determine d_4, the Hartree-like equation (1.4) has been solved for a free semi-infinite system in [18]. For this purpose the external field was set to zero, $U_{sub}(\mathbf{r}) \equiv 0$, and a planar symmetry was imposed $\rho(\mathbf{r}) \equiv \rho(z)$, where z is the coordinate normal to the free surface. In this case the equation (1.4) becomes

$$\left[-\frac{\hbar^2}{2m}\frac{\mathrm{d}^2}{\mathrm{d}z^2} + V_H(z)\right]\sqrt{\rho(z)} = \mu\sqrt{\rho(z)}. \qquad (2.5)$$

The surface energy per unit area σ_s may be obtained by multiplying this Hartree equation with $\mathrm{d}\sqrt{\rho(z)}/\mathrm{d}z$ and integrating twice by using the explicit form (A.2) for $V_H(z) \equiv V_H^{Sky}(z)$

$$\sigma_s = \int_{-\infty}^{\infty}\mathrm{d}z\left[\frac{\hbar^2}{m}\left(\frac{\mathrm{d}\sqrt{\rho(z)}}{\mathrm{d}z}\right)^2 + 2\,d_4\left(\frac{\mathrm{d}\rho(z)}{\mathrm{d}z}\right)^2\right]. \qquad (2.6)$$

The Hartree equation has been iterated until σ_s given by (2.6) was equal to the experimental value $\sigma_s^{expt} = 0.274 \pm 0.003$ K/Å^2 taken from [20], yielding $d_4 = 2.383 \times 10^3$ K Å^5, which was also included in Table 1. It can be readily verified that the evaluation of the integral expressed in equation (2.6) by using this result for d_4 and the values of $\rho(z)$ listed in Table III of [18] leads to the imposed surface tension. It should be mentioned that, as quoted in Table 2, a subsequent measurement [21] led to $\sigma_s^{expt} = 0.2570 \pm 0.0004$ K/Å^2, but a very recent experiment [22] yielded $\sigma_s^{expt} = 0.272 \pm 0.002$ K/Å^2 in complete agreement with the oldest value of [20].

It has been shown that a zero-range force of Skyrme type can provide a reasonable description of thermodynamic properties of the liquid at zero temperature and in the limit of zero momentum. However, in order to describe other properties of the liquid, like the static form factor or the excitation energy spectrum both as a function of momentum, one has to go beyond this limit.

Indeed, the presence of the gradient term implies that the interaction is not really "pure" zero range. Nonlocal terms like $|\nabla\rho(\mathbf{r})|^2$ in (2.1), turn out to be crucial for the description of inhomogeneous liquid helium [18,23]. However, Clements *et al.* [9] pointed out that this kind of gradients terms lead to divergencies when three-dimensional systems approach a two-dimensional geometry. Other current criticism posed on zero-range Skyrme interaction is that it ignores two major characteristics of the interatomic potential: (i) the asymptotic r^{-6} behaviour, and (ii) the hard core repulsion at short distances. This led to the introduction of more elaborated nonlocal density functional (NLDF) formalisms that overcome these shortcomings.

2.2 Orsay-Paris nonlocal density functional

Effects of non-locality have been included in the DF in a more realistic way by Dupont-Roc *et al.* [24]. These authors have replaced the zero-range terms $b_4\rho(\mathbf{r})/2$ and $c_4\rho^{\gamma_4+1}(\mathbf{r})/2$ contributing to the functional (2.1) by nonlocal generalizations of them and discarded the gradient term $d_4|\nabla\rho(\mathbf{r})|^2/\rho(\mathbf{r})$.

The first term of equation (2.1) was replaced by an integrated two-body interaction

$$\frac{b_4}{2}\rho(\mathbf{r}) \to \frac{1}{2}\int \mathrm{d}\mathbf{r}'\,\rho(\mathbf{r}')\,V_1(|\,\mathbf{r}-\mathbf{r}'\,|). \qquad (2.7)$$

In this Orsay-Paris (OP) proposal, $V_1(|\,\mathbf{r}-\mathbf{r}'\,|)$ was taken as the ^{4}He-^{4}He LJ potential screened in a simple way at distances shorter than a characteristic distance h_{OP}

$$V_1^{OP}(r) = \begin{cases} 4\epsilon\left[\left(\frac{\sigma}{r}\right)^{12} - \left(\frac{\sigma}{r}\right)^{6}\right] & \text{if } r \geq h_{OP}, \\ V_1^{OP}(h_{OP})\left(\frac{r}{h_{OP}}\right)^4 & \text{if } r < h_{OP}, \end{cases} \qquad (2.8)$$

with the standard de Boer-Michels [25] parameters, namely, well depth $\epsilon = 10.22$ K and hard core radius $\sigma = 2.556$ Å. In order to recover the correct results for bulk liquid, the screening distance h_{OP} was adjusted so that the integral of $V_1^{OP}(r)$ over the whole three-dimensional

Table 2. Experimental data and coefficients of the expansion for the energy per particle e together with the corresponding reduced χ^2 of each fit.

Data source	e_∞ [K]	$\sigma_\infty = a_1/2$ [K/Å^2]	a_2 [K/Å^4]	$\gamma_c \times 10^3$ [K/Å^6]	$a_4 \times 10^3$ [K/Å^8]	$a_5 \times 10^6$ [K/Å^{10}]	Ref.
Experiment							
e_B	-7.15[a]						[18]
Surface tension		0.274 ± 0.003					[20]
		0.2570 ± 0.0004					[21]
		0.272 ± 0.002					[22]
Theory							
FHH[b]				$\gamma_{frf}^0 = -5.43$			[24], PW
GFMC+VMC	-7.12 ± 0.02	0.288 ± 0.012	-0.021 ± 0.007	$+0.49 \pm 0.42$			[12], PW[c]
	-7.111 ± 0.019	0.275 ± 0.013		-5.7 ± 5.8	$+0.57 \pm 0.94$		PW[d]
	-7.107 ± 0.020	0.270 ± 0.007		-3.52 ± 0.53	$+0.224 \pm 0.041$	-0.8 ± 3.8	PW[d]
Skyrme-DF		0.274[e]					[18]
	-7.154 ± 0.009	0.2760 ± 0.0028		$+0.09 \pm 0.35$	-0.137 ± 0.039		PW
	-7.165 ± 0.008	0.2795 ± 0.0023		$+0.09 \pm 0.35$	-0.244 ± 0.060	12.6 ± 2.9	PW
OP-NLDF		0.277[f]					[24]
	-7.14 ± 0.01	0.278 ± 0.002		-1.3 ± 0.2			[14][g]
	-7.153 ± 0.009	0.2803 ± 0.0027		-1.44 ± 0.33	$+0.009 \pm 0.036$		PW
	-7.157 ± 0.008	0.2815 ± 0.0022		-1.44 ± 0.33	-0.031 ± 0.057	4.8 ± 2.7	PW
C-NLDF		0.287					[30][h]
	-7.154 ± 0.009	0.2875 ± 0.0027		-1.51 ± 0.33	$+0.007 \pm 0.036$		PW
	-7.158 ± 0.008	0.2889 ± 0.0022		-1.51 ± 0.33	-0.037 ± 0.057	5.3 ± 2.7	PW
OT-NLDF		0.272[i]					[31]
	-7.153 ± 0.009	0.2737 ± 0.0028		-1.38 ± 0.36	$+0.014 \pm 0.038$		PW
	-7.155 ± 0.008	0.2745 ± 0.0023		-1.38 ± 0.36	-0.016 ± 0.060	3.8 ± 2.9	PW

[a] Bulk energy per particle quoted in Table II of reference [18] and used for fixing the parameters of all examined DFs, for the error analysis we assumed that the uncertainty of this value is 0.01 K.
[b] Coefficient γ_c estimated by using the FHH approach as explained in text.
[c] Parameters of the fit of all GFMC+VMC data plotted in Figure 3 of reference [12] to equation (3.2) with $a_2 \neq 0$ and $a_k = 0$ for $k \geq 4$.
[d] Parameters of the fit of all GFMC+VMC data plotted in Figure 3 of reference [12] to the fifth-degree polynomial of equation (4.3).
[e] Surface tension quoted in Table II of reference [18] and used therein to fix the parameter d_4 of the Skyrme-DF.
[f] Surface tension evaluated in reference [24] for a rather thick slab by using the OP-NLDF approach.
[g] Parameters determined in reference [14] from a fit of OP-NLDF energy data to equation (4.3) with $a_2 = a_4 = 0$.
[h] Surface tension determined from the analysis of ^{4}He droplets.
[i] Surface tension evaluated in reference [31] for a rather thick slab by using the OT-NLDF approach.

space be equal to the value of b_4 given in Table 1

$$b_4 = \int \mathrm{d}\mathbf{r} V_1^{\mathrm{OP}}(r) = \frac{32\pi}{21}\sigma^3\epsilon\left[\frac{8}{3}\left(\frac{\sigma}{h_{\mathrm{OP}}}\right)^9 - 5\left(\frac{\sigma}{h_{\mathrm{OP}}}\right)^3\right]. \tag{2.9}$$

This procedure led to $h_{\mathrm{OP}} = 2.376\,728$ Å, which is also included in Table 1.

For replacing the second term of equation (2.1), it was used a prescription similar to the "weighted density approximation" introduced in the studies of classical fluids by Tarazona [26]

$$\frac{c_4}{2}\,\rho^{\gamma_4+1}(\mathbf{r}) \to \frac{c_4}{2}\,[\bar{\rho}(\mathbf{r})]^{\gamma_4+1}. \tag{2.10}$$

The $\bar{\rho}(\mathbf{r})$ is the "coarse-grained density" defined as the straight average of $\rho(\mathbf{r})$ over a sphere centered at $\mathbf{r}$ and with a radius equal to the screening distance h_{OP}

$$\bar{\rho}(\mathbf{r}) = \int \mathrm{d}\mathbf{r}'\,\rho(\mathbf{r}')\,\mathcal{W}(|\,\mathbf{r}-\mathbf{r}'\,|), \tag{2.11}$$

where $\mathcal{W}(|\,\mathbf{r}-\mathbf{r}'\,|)$ is the normalized step function

$$\mathcal{W}(|\,\mathbf{r}-\mathbf{r}'\,|) = \frac{3}{4\pi h^3}\,\Theta(\,h - |\,\mathbf{r}-\mathbf{r}'\,|) = \begin{cases} \dfrac{3}{4\pi h^3} & \text{if } |\,\mathbf{r}-\mathbf{r}'\,| \leq h, \\ 0 & \text{if } |\,\mathbf{r}-\mathbf{r}'\,| > h. \end{cases} \tag{2.12}$$

The OP-NLDF expression for the correlation energy per particle suggested by Dupont-Roc and collaborators

$$e_c^{\mathrm{OP}}(\mathbf{r}) = \frac{1}{2}\int \mathrm{d}\mathbf{r}'\,\rho(\mathbf{r}')\,V_1^{\mathrm{OP}}(|\,\mathbf{r}-\mathbf{r}'\,|) + \frac{c_4}{2}\,[\,\bar{\rho}(\mathbf{r})\,]^{\gamma_4+1}, \tag{2.13}$$

combines the simplicity of the zero-range one with the possibility of obtaining a reasonable result for the surface tension of the liquid without explicit inclusion of gradient terms in e_c (see, *e.g.*, the value $\sigma_s = 0.277$ K/Å^2 of equation (28) in [24]).

Finally, in this approach it is also interesting to look at the prediction for the static response function $\chi(q, \omega = 0)$ of uniform ^{4}He liquid at zero pressure given by

$$-\chi^{-1}(q) = \frac{\hbar^2 q^2}{4m} + \frac{\rho_0}{V} \iint d\mathbf{r}\, d\mathbf{r}' \frac{\delta^2 E_c[\rho]}{\delta\rho(\mathbf{r})\, \delta\rho(\mathbf{r}')} e^{-i\,\mathbf{q}\cdot(\mathbf{r}-\mathbf{r}')} = \frac{\hbar^2 q^2}{4m} + \rho_0 \hat{V}_1(q) + (\gamma_4 + 1) c_4 \rho_0^{\gamma_4+1} \left[\hat{\mathcal{W}}(q) + \frac{\gamma_4}{2} \hat{\mathcal{W}}^2(q) \right], \quad (2.14)$$

where $\rho_0 = 0.021\,836$ Å^{-3} is the equilibrium density and the functions $\hat{f}(q)$ are the Fourier transforms

$$\hat{f}(q) = \int d\mathbf{r}\, f(|\,\mathbf{r}\,|)\, e^{-i\,\mathbf{q}\cdot\mathbf{r}}. \quad (2.15)$$

In particular, the Fourier transform of $\mathcal{W}(|\,\mathbf{r} - \mathbf{r}'\,|)$ yields

$$\hat{\mathcal{W}}(q) = \int d\mathbf{r}\, \mathcal{W}(|\,\mathbf{r} - \mathbf{r}'\,|)\, e^{-i\,\mathbf{q}\cdot\mathbf{r}} = \frac{3}{h\,q}\, j_1(h\,q) = \frac{3}{h^2 q^2} \left[\frac{\sin(h\,q)}{h\,q} - \cos(h\,q) \right]. \quad (2.16)$$

The static polarizability of ^{4}He, in units of its value at zero momentum which is fixed by the compressibility of the system $-\chi^{-1}(q = 0) = 1/\rho_0\,\kappa_v = 27.2$ K, is shown in Figure 1 of [24] together with experimental data from [27]. The theoretical results reproduce approximately the measured values, except at the valley of the roton region ($q \simeq 2$ Å^{-1}).

2.3 Catalonia nonlocal density functional

An alternative finite-range DF has been built by Barranco *et al.* [28] starting from the proposal of [24] and merely changing the treatment of the hard core of the LJ potential. Following the idea of Pines' polarization potentials [29], the authors of [28] suggested the interaction

$$V_1^C(r) = \begin{cases} 4\epsilon \left[\left(\frac{\sigma}{r}\right)^{12} - \left(\frac{\sigma}{r}\right)^{6} \right] & \text{if } r \geq \sigma, \\ b_{LJ} \left[1 - \left(\frac{r}{\sigma}\right)^{8} \right] & \text{if } r < \sigma, \end{cases} \quad (2.17)$$

where ϵ and σ are the standard de Boer-Michels parameters. The height b_{LJ} of the core is fixed so that the results for the bulk liquid be recovered. In so doing, from

$$b_4 = \int d\mathbf{r}\, V_1^C(r) = \frac{32\,\pi}{3}\,\sigma^3 \left[\frac{1}{11}\, b_{LJ} - \frac{1}{3}\,\epsilon \right], \quad (2.18)$$

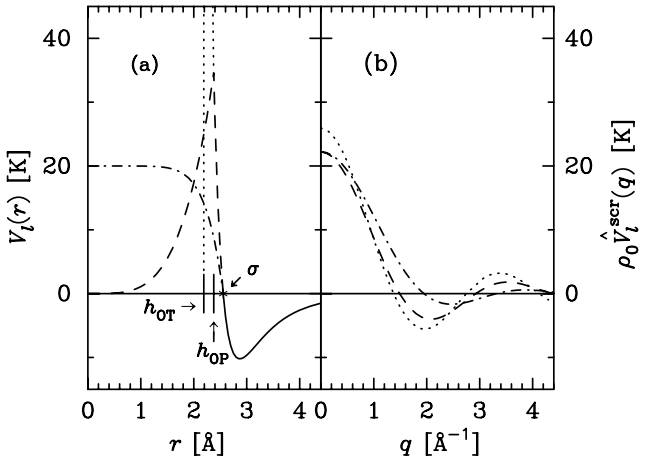

Fig. 1. (a) Screened portions of the Lennard-Jones potentials as a function of the inter-particle distance. The full curve indicates the common unscreened part of the potential. The dashed curve shows the short-range sector adopted in the OP-NLDF approach of [24]. The dot-dashed curve is the short-range C-NLDF polarization potential introduced in [28]. For the sake of comparison the Orsay-Trento screening of [31] is also marked schematically by dotted lines. (b) Contributions to $\rho_0 \hat{V}_1(q)$ evaluated by using equation (2.21) with the corresponding screened potentials $V_1(r \leq \sigma)$ displayed in part (a).

the following relation was obtained

$$b_{LJ} = \frac{33}{8} \left[\frac{8}{9}\,\epsilon + \frac{b_4}{4\,\pi\,\sigma^3} \right]. \quad (2.19)$$

Figure 1 shows the difference between the screening at short-range of the potentials adopted in [24] and [28]. All the remaining phenomenological parameters of this Catalonia finite-range DF (C-NLDF) are the same as those of the OP-NLDF. In the C-NLDF approach for the correlation energy per particle reads

$$e_c^C(\mathbf{r}) = \frac{1}{2} \int d\mathbf{r}'\, \rho(\mathbf{r}')\, V_1^C(|\,\mathbf{r} - \mathbf{r}'\,|) + \frac{c_4}{2}\, [\,\bar{\rho}(\mathbf{r})\,]^{\gamma_4+1}. \quad (2.20)$$

The distance $h_C = h_{OP}$ is only used as the cut-off for the determination of $\bar{\rho}(\mathbf{r})$.

The static polarizability of ^{4}He obtained with the C-NLDF approximation is shown in Figure 2 of [30] together with the results of [24] and the experimental data of [27]. From this comparison one realizes that both OP- and C-NLDF proposals provide similar results, this is due to fact that the difference between contributions yielded to $\hat{V}_1(q)$ by different screenings in $V_1(r)$ for $r \leq \sigma$, *i.e.*,

$$\hat{V}_1^{scr}(q) = \frac{4\,\pi}{q} \int_0^\sigma dr\, r\, V_1(r)\, \sin(qr), \quad (2.21)$$

is not significant as can be seen in Figure 1.

In the literature [9], it has been claimed that approaches such as OP- and C-NLDF do not reproduce the two-dimensional equation of state. It has been consequently attributed to this deficiency that systems with

two-dimensional substructures like layers or shells cannot be correctly described by these semi-phenomenological theories. Furthermore, it has been argued that just due to this failure these NLDFs are not able to account for growing instabilities like that found in CBF-HNC calculations [8] for ^{4}He films adsorbed on strongly enough substrates.

2.4 Orsay-Trento nonlocal density functional

Dalfovo *et al.* [31] have devised a functional by making minor modifications in the terms contributing to equation (2.13), but introducing a new term for getting an accurate description of the static response function. The height of the peak of $\chi(q)$ in the roton region, $q \simeq 2$ Å^{-1}, is important in characterizing structural properties on the interatomic length scale (for instance, the layered structure of helium films). Therefore, the idea of Dalfovo *et al.* [31] has been to improve on the previous NLDF approaches in order to better reproduce the experimental peak of $\chi(q)$ in the roton region.

In this case the two-body interaction was taken as the LJ potential with a truncated core

$$V_{\rm l}^{\rm OT}(r) = \begin{cases} 4\epsilon \left[\left(\frac{\sigma}{r}\right)^{12} - \left(\frac{\sigma}{r}\right)^{6} \right] & \text{if } r \geq h_{\rm OT}, \\ 0 & \text{if } r < h_{\rm OT}. \end{cases} \tag{2.22}$$

Now the integral of the screened LJ potential gives

$$b_4' = \int {\rm d}\mathbf{r}\, V_{\rm l}^{\rm OT}(r) = \frac{16\pi}{3}\sigma^3\epsilon \left[\frac{1}{3}\left(\frac{\sigma}{h_{\rm OT}}\right)^9 - \left(\frac{\sigma}{h_{\rm OT}}\right)^3 \right]. \tag{2.23}$$

The contribution depending on $\bar{\rho}(\mathbf{r})$ was split into two terms

$$\frac{c_4}{2}\,[\,\bar{\rho}(\mathbf{r})\,]^{\gamma_4+1} \rightarrow \frac{c_4'}{2}\,[\,\bar{\rho}(\mathbf{r})\,]^2 + \frac{c_4''}{3}\,[\,\bar{\rho}(\mathbf{r})\,]^3. \tag{2.24}$$

In order to reproduce correctly the behaviour of $\chi(q)$ it was added a contribution $e_{\rm gg}[\nabla\rho]$, which depends on the gradient of the density at different points and corresponds to a nonlocal correction to the kinetic energy. So that the whole Orsay-Trento functional (OT-NLDF) reads

$$e_{\rm c}^{\rm OT}(\mathbf{r}) = \frac{1}{2}\int {\rm d}\mathbf{r}'\,\rho(\mathbf{r}')\,V_{\rm l}^{\rm OT}(\mid \mathbf{r}-\mathbf{r}'\mid) + \frac{c_4'}{2}\,[\,\bar{\rho}(\mathbf{r})\,]^2 + \frac{c_4''}{3}\,[\,\bar{\rho}(\mathbf{r})\,]^3 + e_{\rm gg}[\nabla\rho]. \tag{2.25}$$

As in the case of the zero-range DF the parameters b_4', c_4', and c_4'' were adjusted to reproduce data at equilibrium of saturated homogeneous liquid. The uniform limit of the OT-NLDF expression for the correlation energy per particle is

$$e_{\rm u} = \frac{E}{N} = \frac{b_4'}{2}\,\rho + \frac{c_4'}{2}\,\rho^2 + \frac{c_4''}{3}\,\rho^3. \tag{2.26}$$

The corresponding formulas for pressure and compressibility may be derived by using the definitions of equations (2.3) and (2.4). The relevant observables at saturation, *i.e.*, the equilibrium density, the minimum energy per particle, and the compressibility are correctly reproduced by the set of parameters b_4', c_4', and c_4'' listed in Table 1. The screening distance $h_{\rm OT} = 2.190\,323$ Å, obtained from equation (2.23) by using this value of b_4' is also quoted in that table.

The complete OT-NLDF [31] expression for the gradient-gradient contribution is

$$e_{\rm gg}[\nabla\rho] = -\frac{\hbar^2}{4\,m}\,\alpha_{\rm s}\int {\rm d}\mathbf{r}'\,\rho(\mathbf{r}')F(\mid \mathbf{r}-\mathbf{r}'\mid)\left[1-\frac{\widetilde{\rho}(\mathbf{r})}{\rho_{0s}}\right] \times \left(\frac{\nabla\rho(\mathbf{r})}{\rho(\mathbf{r})}\right)\cdot\left(\frac{\nabla\rho(\mathbf{r}')}{\rho(\mathbf{r}')}\right)\left[1-\frac{\widetilde{\rho}(\mathbf{r}')}{\rho_{0s}}\right], \tag{2.27}$$

where $\widetilde{\rho}(\mathbf{r})$ is a weighted average of the one-body density

$$\widetilde{\rho}(\mathbf{r}) = \int {\rm d}\mathbf{r}'\,\rho(\mathbf{r}')\,F(\mid \mathbf{r}-\mathbf{r}'\mid), \tag{2.28}$$

and $F(\mid \mathbf{r}-\mathbf{r}'\mid)$ is a Gaussian weighting function

$$F(\mid \mathbf{r}-\mathbf{r}'\mid) = \frac{1}{\pi^{3/2}\,\ell^3}\,{\rm e}^{-|\mathbf{r}-\mathbf{r}'|^2/\ell^2}. \tag{2.29}$$

Dalfovo *et al.* [31] emphasized that this expression for $e_{\rm gg}[\nabla\rho]$ is required for studying films adsorbed on strongly attractive substrates, while for investigating free surface, helium clusters, and films on weak binding substrates is enough to use a simplified version of $e_{\rm gg}[\nabla\rho]$ given in the Appendix B of [32], where $\widetilde{\rho}(\mathbf{r}) \equiv \rho(\mathbf{r})$.

The new phenomenological parameters $\alpha_{\rm s}$, ρ_{0s}, and ℓ were fixed to reproduce the peak of $\chi(q)$ in the bulk liquid. In this approach, the formula for the static response function at zero pressure derived by using the definition of equation (2.14) is

$$-\chi^{-1}(q) = \frac{\hbar^2\,q^2}{4\,m} + \rho_0\,\hat{V}_{\rm l}(q) + c_4'\,\rho_0^2\left[2\,\hat{\mathcal{W}}(q) + \hat{\mathcal{W}}^2(q)\right] + 2\,c_4''\,\rho_0^3\left[\hat{\mathcal{W}}(q) + \hat{\mathcal{W}}^2(q)\right] - \frac{\hbar^2}{2\,m}\,\alpha_{\rm s}\,\rho_0\left(1-\frac{\rho_0}{\rho_{0s}}\right)^2 q^2\,{\rm e}^{-q^2\ell^2/4}. \tag{2.30}$$

The obtained values of $\alpha_{\rm s}$, ρ_{0s}, and ℓ are given in Table 1. The $\chi(q)$ calculated by using equation (2.30) are displayed in Figure 1 of [31] showing an excellent agreement with the experimental data of [27].

In order to complete the comparison among the contributions provided by different screenings of the LJ potential, we also evaluated $\hat{V}_{\rm l}^{\rm scr}(q)$ for this OT-NLDF. The result is plotted in Figure 1 and indicates that the differences with previous approaches are not very important.

3 The case of planar symmetry

When the external potential depends only on the coordinate z normal to the surface, *i.e.*, $U_{\rm sub}(\mathbf{r}) \equiv U_{\rm sub}(z)$, the Hartree-like equation (1.4) takes the form (2.5). Under such conditions the system exhibits a planar symmetry for which the one-body density satisfies $\rho(\mathbf{r}) \equiv \rho(z)$. For this geometry, it is useful to define the surface coverage as the number of particles per unit area

$$n_{\rm c} = \frac{N}{A} = \int_{-\infty}^{\infty} {\rm d}z\, \rho(z). \tag{3.1}$$

3.1 Energy per particle as a function of coverage

Since in the present work we shall focus the attention on free slabs of liquid ^{4}He, the external field is taken to be zero, $U_{\rm sub}(z) \equiv 0$. Consequently the density profile $\rho(z)$ determined from solutions of the Hartree-like equation (2.5) is symmetric at $z = 0$. For this geometry the energy per particle becomes

$$e = \frac{E_{\rm gs}}{N} = \frac{1}{n_{\rm c}} \left[\frac{\hbar^2}{2m} \int_{-\infty}^{\infty} {\rm d}z \left(\frac{{\rm d}\sqrt{\rho(z)}}{{\rm d}z} \right)^2 + \int_{-\infty}^{\infty} {\rm d}z\, \rho(z)\, e_{\rm c}(z) \right]. \tag{3.2}$$

The expressions for the correlation energy per particle, $e_{\rm c}(z)$, provided by each one of the different DF approaches discussed above are given in the Appendix.

3.2 Treatment of the energetics

The energetics of free planar films of ^{4}He was analyzed by using an improved version of the formalism adopted in a previous paper [14] for studying the instability of these systems. Following the formulation devised in [33] we shall assume that the energy per particle may be approximated by a polynomial expansion in powers of the inverse of coverage

$$e = \frac{E_{\rm gs}}{N} = e_\infty + \sum_{k=1}^{\infty} \frac{a_k}{n_{\rm c}^k}\,. \tag{3.3}$$

In fact, this parameterization is similar to that introduced in [34] for the free energy in terms of film's thickness. Here the energy per particle in the limit $n_{\rm c} \to \infty$, *i.e.*, e_∞, can be identified with $e_{\rm B}$. The physical content of the coefficients a_k may be obtained from thermodynamic considerations.

For a single-component system of N particles which presents a volume V and a surface of area A, the ground-state energy at $T = 0$ K satisfies according to (2.11) of [35]

$${\rm d}E_{\rm gs} = -P\, {\rm d}V + \sigma_A\, {\rm d}A + \mu\, {\rm d}N. \tag{3.4}$$

The intensive thermodynamic fields P, σ_A, and μ are pressure, surface tension and chemical potential, respectively. Since in the case of flat interfaces at $T = 0$ K the pressure P is zero, equation (3.4) reduces to

$${\rm d}E_{\rm gs} = \sigma_A\, {\rm d}A + \mu\, {\rm d}N. \tag{3.5}$$

The formal thermodynamic definitions of σ_A and μ lead to the following expressions in terms of the energy per particle e

$$\sigma_A = \left(\frac{\partial E_{\rm gs}}{\partial A} \right)_N = \left(\frac{\partial (E_{\rm gs}/N)}{\partial (A/N)} \right)_N = -\, n_{\rm c}^2\, \frac{\partial e}{\partial n_{\rm c}}, \tag{3.6}$$

and

$$\mu = \left(\frac{\partial E_{\rm gs}}{\partial N} \right)_A = \left(\frac{\partial (E_{\rm gs}/A)}{\partial (N/A)} \right)_A = e + n_{\rm c}\, \frac{\partial e}{\partial n_{\rm c}}\,. \tag{3.7}$$

From these equations one gets the well-known relation

$$\sigma_A = n_{\rm c}\, (\, e - \mu\,) = \frac{E_{\rm gs}}{A} - \mu\, n_{\rm c}. \tag{3.8}$$

The chemical potential derived by using equations (3.3) and (3.7) becomes

$$\mu = e_\infty - \sum_{k=2}^{\infty} (k-1) \frac{a_k}{n_{\rm c}^k}, \tag{3.9}$$

being independent of a_1. A further simplification can be achieved for films adsorbed on substrates occupying the half-space $z < 0$. In such a case, for thick enough slabs only the van der Waals tail of the substrate-adsorbate potential, which is proportional to z^{-3}, is relevant for the growth of the system. In particular, it was shown in [36] that for standard "3-9" potentials of the form

$$U_{\rm sub}(z) = \frac{4}{27\, D^2} \left(\frac{C_3}{z^3} \right)^3 - \frac{C_3}{z^3}, \tag{3.10}$$

in the large coverage regime the chemical potential varies to first-order approximation as $1/d^3$ (d being the film's thickness)

$$\mu \simeq e_\infty - \frac{\Gamma}{d^3}\,. \tag{3.11}$$

Quantity Γ is mainly determined by C_3 and for films filling up the $z \geq 0$ region d is usually defined in terms of the equilibrium bulk density ρ_0 as

$$d = \frac{1}{\rho_0} \int_0^{\infty} {\rm d}z\, \rho(z). \tag{3.12}$$

According to the simplest version of the Frenkel-Halsay-Hill (FHH) model, see *e.g.* equation (5) of [36] which has been derived by neglecting effects due to retardation of the van der Waals force, Γ is directly determined by the strength of the long-range tail of the interaction between ^{4}He and the substrate

$$\Gamma \simeq \Gamma_{\rm FHH} = \Delta C_3 \equiv C_3 - C_3^{\rm He}, \tag{3.13}$$

with $C_3^{\rm He}$ being the C_3 coefficient of a hypothetical ^{4}He substrate. It seems plausible to extend this result to thick free films assuming that in absence of attractive substrates, *i.e.*, in the limit $C_3 \to 0$, the $\Gamma_{\rm frs}$ corresponding to a free planar surface of liquid helium would be mainly determined by $C_3^{\rm He}$. An expression for the latter quantity has been derived by Dupont-Roc and collaborators in the limiting case of a semi-infinite system of ^{4}He. By starting from the $V_{\rm H}(z)$ potential these authors showed that the relevant term, which is common to all the above described NLDF approaches, leads to equation (22) of [24] where

$$C_3^{\rm He} \simeq \frac{2}{3}\,\pi\,\epsilon\,\sigma^6\,\rho_0 \simeq 130\ {\rm K\,\mathring{A}}^3. \tag{3.14}$$

This value of $C_3^{\rm He}$ should be appropriate to account for long-range effects due to thick half-slabs of the type of that plotted in Figures 1 and 2 of [12]. In the case of such films the half-coverage $n_{1/2}$ satisfies

$$n_{1/2} = \int_0^\infty {\rm d}z\ \rho(z) = \rho_0\, d. \tag{3.15}$$

Hence, for large systems of this kind, according to equations (3.11–3.14) the chemical potential could be approximated by

$$\mu \simeq e_\infty + C_3^{\rm He}\,\rho_0^3\,\frac{1}{n_{1/2}^3}\cdot \tag{3.16}$$

This expression can be derived by applying the definition of equation (3.7) to an expansion for the energy per particle similar to that of equation (2) in [37]

$$e \simeq e_\infty + \frac{a_1'}{n_{1/2}} + \frac{a_3'}{n_{1/2}^3}, \tag{3.17}$$

where $a_2' = 0$ is explicitly assumed and a_3' should satisfy

$$a_3' \simeq -\,\frac{1}{2}\,C_3^{\rm He}\,\rho_0^3. \tag{3.18}$$

In fact, the expansion in powers of $1/n_{1/2}$ written in equation (3.17) is just of the type of equation (5) of [12], which has been used therein to study the energetics of half-slabs. As pointed out in [14], since $n_{1/2} = n_{\rm c}/2$ the relation between the coefficients of the terms of order m in the expansions of equations (3.3) and (3.17) is $a_k = 2^k\,a_k'$. In particular, from the comparison of these expressions one concludes that the coefficient a_2 should be zero. So the chemical potential of equation (3.9) may be rewritten as

$$\mu = e_\infty - 2\,\frac{\gamma_{\rm c}}{n_{\rm c}^3} - \sum_{k=4}^{\infty}(k-1)\,\frac{a_k}{n_{\rm c}^k}, \tag{3.19}$$

where we have separated explicitly the main contribution due to the van der Waals tail and renamed the coefficient a_3 as

$$a_3 \equiv \gamma_{\rm c}. \tag{3.20}$$

The derivation of the surface tension by applying equation (3.6) to the expansion (3.3) leads to

$$\sigma_A = a_1 + 3\,\frac{\gamma_{\rm c}}{n_{\rm c}^2} + \sum_{k=4}^{\infty} k\,\frac{a_k}{n_{\rm c}^{k-1}}, \tag{3.21}$$

where, as above, it was set $a_2 = 0$. The coefficient a_1 may be identified with the total surface tension in the limit of infinite width

$$a_1 = \lim_{n_{\rm c}\to\infty} \sigma_A = \sigma_\infty^{\rm (tot)}. \tag{3.22}$$

Since a planar symmetric film has two equivalent surfaces, the surface tension at each boarder, $\sigma_{\rm s}$, is a half of the total σ_A. Hence we may write

$$\sigma_{\rm s} = \frac{\sigma_A}{2} = \sigma_\infty + \frac{3}{2}\,\frac{\gamma_{\rm c}}{n_{\rm c}^2} + \frac{1}{2}\,\sum_{k=4}^{\infty} k\,\frac{a_k}{n_{\rm c}^{k-1}}, \tag{3.23}$$

where $\sigma_\infty = \sigma_\infty^{\rm (tot)}/2$ is the surface tension of a semi-infinite system.

For the sake of completeness, we shall remark that the information concerning the stability of the films is carried by $\gamma_{\rm c}$ and the coefficients of higher-order terms. As pointed out in [14], a suitable criterion for ensuring the stability of a system is to require a positive areal isothermal compressibility $\kappa_{\rm s}$. At $T = 0$ K this condition may be formulated in the following way

$$\frac{1}{\kappa_{\rm s}} = A\left(\frac{\partial\sigma_A}{\partial A}\right)_N = \frac{A}{N}\left(\frac{\partial\sigma_A}{\partial(A/N)}\right)_N = -n_{\rm c}\frac{\partial\sigma_A}{\partial n_{\rm c}} > 0. \tag{3.24}$$

It may be rewritten in terms of the incompressibility, which has the dimension of an energy and is related to the third-sound velocity c_3

$$\begin{aligned}\frac{1}{n_{\rm c}\,\kappa_{\rm s}} &= -\,\frac{\partial\sigma_A}{\partial n_{\rm c}} = n_{\rm c}\,\frac{\partial\mu}{\partial n_{\rm c}} = m\,c_3^2 \\ &= 6\,\frac{\gamma_{\rm c}}{n_{\rm c}^3} + \sum_{k=4}^{\infty} k(k-1)\,\frac{a_k}{n_{\rm c}^k} > 0.\end{aligned} \tag{3.25}$$

It is worthwhile to stress that the incompressibility is independent of the quantities e_∞ and σ_∞, it depends on how the chemical potential and the surface tension reach these asymptotic values. Therefore, it is of interest to estimate the magnitude of $\gamma_{\rm c}$ which for thick species should govern the leading contribution to $1/(n_{\rm c}\,\kappa_{\rm s})$. An approximated size of $\gamma_{\rm c}$ for free films may be estimated by taking into account equations (3.14) and (3.18)

$$\begin{aligned}\gamma_{\rm c} = a_3 = 8\,a_3' &\simeq -\,4\,C_3^{\rm He}\,\rho_0^3 \simeq -\,\frac{8}{3}\,\pi\,\epsilon\,\sigma^6\,\rho_0^4 \\ &= -\,5.43\times10^{-3}\ {\rm K\,\mathring{A}}^{-6} = \gamma_{\rm frf}^0.\end{aligned} \tag{3.26}$$

After taking into account abovementioned facts, the energy per particle may be written as

$$e = e_\infty + 2\,\frac{\sigma_\infty}{n_{\rm c}} + \frac{\gamma_{\rm c}}{n_{\rm c}^3} + \sum_{k=4}^{\infty}\frac{a_k}{n_{\rm c}^k}\cdot \tag{3.27}$$

4 Numerical results

Let us now compare the outputs for free films obtained from calculations carried out with DF approaches and MC simulations. We shall pay attention to results for several relevant quantities. Namely, the energy per particle e, the surface tension σ_s, the density at the centre of the films ρ_c, the half-film thickness $z_{1/2}$, and the surface width W will be examined. The central density is simply $\rho_c = \rho(z = 0)$, the half-film thickness $z_{1/2}$ is defined as the distance from the centre at which the one-body density $\rho(z)$ reaches the value $\rho(z_{1/2}) = \rho_c/2$. Finally, the width W of the liquid-vacuum interface is defined as the distance in which $\rho(z)$ decreases from $0.9\,\rho_c$ to $0.1\,\rho_c$.

4.1 Monte Carlo data

Vallés and Schmidt [12] have performed the MC computations for free slabs of liquid ^{4}He at $T = 0$ K using the semi-empirical improved Hartree-Fock dispersion helium potential of [10] to describe the ^{4}He -^{4}He interaction. Two different techniques, the Green's function Monte Carlo (GFMC) and the variational Monte Carlo (VMC), were utilized for these calculations. In the latter case, two- and three-body factors were included as outlined in [38,39]. The simulation area was taken to be $A_{MC} = 580.6$ Å^2. Both series of data for e listed in Table I of [12] are given as a function of N_{MC} which is the number of particles in a half of a symmetric film (*cf.* Figs. 1 and 2 therein). However, in order to facilitate the forthcoming study, for which we shall utilize the formulas reported in the previous section, it is convenient to consider the total coverage $n_c = 2\,N_{MC}/A_{MC}$. Both MC series of data may be supplemented by including values calculated for infinite system, *i.e.*, $e_\infty(\mathrm{GFMC}) = -7.12 \pm 0.02$ K (GFMC from [40]) and $e_\infty(\mathrm{VMC}) = -6.69 \pm 0.02$ K (VMC result obtained for a bulk ^{4}He system with $N = 324$ in [12]). Since VMC data exhibit systematic deviations from the GFMC ones, Vallés and Schmidt corrected the former values shifting them by $e_\infty(\mathrm{GFMC}) - e_\infty(\mathrm{VMC})$ (*cf.* Fig. 3 in [12]). Figure 2 shows all GFMC and the corrected VMC data as a function of the inverse of total coverage.

The definitions of the surface tension given by equations (3) and (4) of the paper by Vallés and Schmidt [12] are different from that of equation (3.8). However, due to the fact that equation (3) of [12], *i.e.*,

$$\sigma_1 = \frac{N_{MC}}{A}\,[\,e - e_\infty\,] = \frac{n_c}{2}\,[\,e - \mu_\infty\,], \qquad (4.1)$$

may be also evaluated with the output of DF calculations by introducing the asymptotic value $\mu_\infty = e_\infty$ instead of $\mu(n_c)$ in equation (3.8), it is possible to make meaningful comparisons. The MC data of σ_1 taken from Table I of [12] are plotted in Figure 3. The error bars were estimated in the present work by using the standard deviations of the contributing energies per particle. The observables describing the structure of the films like the half-film thickness $z_{1/2}$ and the surface width W are also listed in Table I of [12].

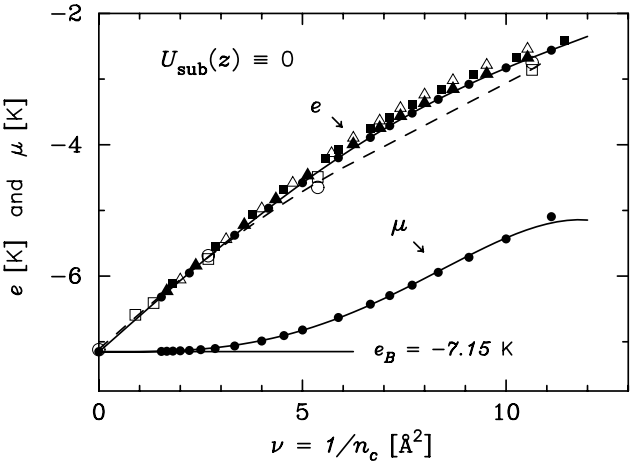

Fig. 2. Comparison of energy per particle as a function of the inverse of total coverage $\nu = 1/n_c$. Open squares and circles are VMC and GFMC data obtained by Vallés and Schmidt [12]. Note that the VMC values are shifted by $e_\infty(\mathrm{GFMC}) - e_\infty(\mathrm{VMC})$ as in Figure 3 of [12]. Results calculated with the Skyrme-DF are represented by open triangles. Full triangles, squares, and circles stand for e provided by the OP-, C-, and OT-NLDF approaches, respectively. In addition, the chemical potential μ yielded by solutions of equation (2.5) with the OT-NLDF Hartree-like potential is also indicated by full circles. Solid curves show e and μ evaluated with equations (4.3) and (3.19) by using the coefficients determined in OT-NLDF case, while the dashed curve indicates the fit of MC data.

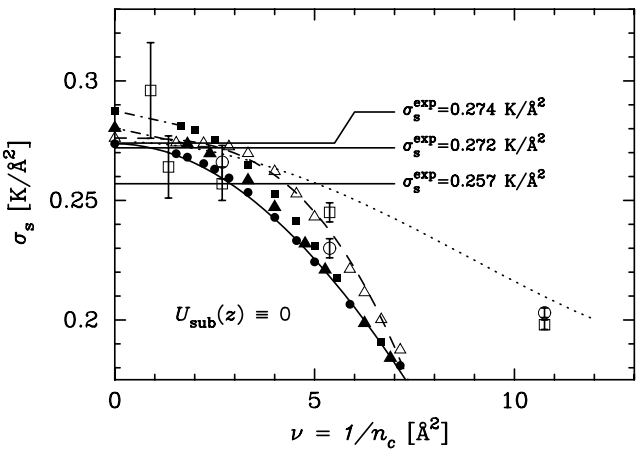

Fig. 3. Comparison of surface tension as a function of the inverse of the coverage $\nu = 1/n_c$. Open squares and circles are VMC and GFMC values of γ_1 taken from Table I of reference [12], the evaluation of the corresponding uncertainties is explained in the text. Results calculated with the Skyrme-DF are represented by open triangles. Full triangles, squares, and circles stand for e provided by the OP-, C-, and OT-NLDF approaches, respectively. In these cases the largest uncertainties are of the size of the symbols. The solid and dashed curves indicate the estimation by using equation (4.4) with the coefficients obtained within the OT-NLDF and Skyrme-DF formalisms, respectively, when data for $n_c \leq 0.13$ Å^{-2} were taken into account. The dotted curve shows the results evaluated for σ_1 in the case of the OT-NLDF.

4.2 Density-functional data

For getting the values of the quantities of interest for free planar films provided by the DF approaches described above, one has to solve the Hartree-like equation given by equation (2.5). The expressions for the Hartree mean-field potential, $V_{\rm H}(z)$, corresponding to each one of the different DF approaches are provided in the Appendix. The integrodifferential problem (2.5) has been solved for a large domain of coverages. The thicker species up to $n_{\rm c} = 0.65$ Å^{-2} were evaluated in order to fill up the regime between the largest film studied with the GFMC technique and the largest ones computed with the VMC method. Selected DF results for e are displayed in Figure 2 together with all the MC data treated as described above. The behaviour of the chemical potential is illustrated by showing in Figure 2 values obtained with the complete OT-NLDF formalism.

Having determined e and μ from solutions of equation (2.5), we evaluated the surface tension $\sigma_{\rm s}$ as a function of coverage by using equation (3.8)

$$\sigma_{\rm s} = \frac{\sigma_A}{2} = \frac{n_{\rm c}}{2}\,[\,e - \mu\,]. \tag{4.2}$$

In addition, σ_1 was also estimated in the case of OT-NLDF. All these results are plotted in Figure 3. On the other hand, the quantities characterizing the structure of the films, *i.e.*, $\rho_{\rm c}$, $z_{1/2}$, and W, were also determined in the present work at several coverages.

4.3 Analysis and discussion

All the series of energy per particle displayed in Figure 2 decrease monotonically for increasing $n_{\rm c}$ and tend towards the value $e_{\rm B}$ in the limit $\nu = 1/n_{\rm c} \to 0$. Of course, this behaviour is to be expected in the case of DFs because the parameters of these semi-phenomenological approaches are adjusted to reproduce saturation properties of the bulk. It becomes clear from this figure that at large coverages, *i.e.*, at small ν, the agreement between DF and MC data is excellent. Small differences appear for $\nu \gtrsim 5$ Å^2, where the energy values calculated with DF formalisms lie systematically slightly above the MC results. Each set of $e(n_{\rm c})$ was fitted to the polynomial given by equation (3.27), where at most terms up to fifth-degree have been retained

$$e = e_\infty + 2\,\frac{\sigma_\infty}{n_{\rm c}} + \frac{\gamma_{\rm c}}{n_{\rm c}^3} + \frac{a_4}{n_{\rm c}^4} + \frac{a_5}{n_{\rm c}^5}\,\cdot \tag{4.3}$$

In practice, the data covering the range $0 \le \nu \lesssim 11$ Å^2 (*i.e.*, also including the value corresponding to bulk liquid) were analyzed in two steps. Firstly, we fitted data of systems with $\rho_{\rm c} > 0.75\,\rho_0 \simeq \rho_{\rm 3D}^{\rm sp}$ to equation (4.3) setting $a_5 = 0$. Since the quantity $\rho_{\rm 3D}^{\rm sp} \simeq 0.16$ Å^{-3} is the spinodal density of bulk liquid (see, *e.g.*, Ref. [13]), the parameters determined with this procedure should account for properties of thick slabs. The results listed Table 3 indicate that species with $n_{\rm c} \ge 0.13$ Å^{-2} satisfy the required condition. In the second step, all data were fitted to the complete polynomial (4.3) with the restriction that $\gamma_{\rm c}$ has been allowed to vary only between the limits determined for each approach in the first adjustment. This kind of fit was performed by using Monte Carlo techniques. For the error analysis of the coefficients obtained from the MC energies per particle we used the standard deviation 0.03 K quoted in Table I of [12]. In the case of the DF approaches the error of energies per particle was assumed to be similar to the uncertainty in the determination of $e_{\rm B}$, *i.e.*, 0.01 K. The extracted values of e_∞, σ_∞, $\gamma_{\rm c}$, a_4, and a_5 are listed in Table 2. All the results for e_∞ are consistent with $e_{\rm B}$. The values of σ_∞ may be compared with experimental data of the surface tension which are also quoted in Table 2. Figure 2 shows the fits for MC and OT-NLDF energy data. This drawing also shows that for the OT-NLDF the chemical potential evaluated by using equation (3.19) reproduces satisfactorily well the values of μ obtained from the solution of equation (2.5). In the following lines we shall discuss in detail the results obtained with the different approaches.

Let us first focus our attention on the results provided by the GFMC + VMC data. It should be stressed that in the original study performed in [12] the term $a_2/n_{\rm c}^2$ was retained and the coefficients a_4 and a_5 were set at zero, while in the present analysis, on the basis of theoretical grounds outlined in Section 3.2, we assumed $a_2 = 0$ and left free a_4 and a_5. The coefficients extracted by Vallés and Schmidt are also given in Table 2. The χ^2 over the degree of freedom $n_{\rm f}$ obtained in the present work from the fit of all the MC data to the complete equation (4.3), $\chi^2/n_{\rm f} \simeq 5$, is large and equivalent to that of [12,14]. However, the parameters determined in the current analysis are more satisfactory than the previous ones. The present surface tension $\sigma_\infty({\rm MC}) = 0.272 \pm 0.008$ K/Å^2 is in much better agreement with experimental data of [20,22] than

Table 3. Central density $\rho_{\rm c}$ and half-film thickness $z_{1/2}$.

$n_{\rm c}$ [Å^{-2}]	ν [Å^2]	$\rho_{\rm c}$ [Å^{-3}]	$z_{1/2}$ [Å]		
		OT-NLDF	OT-NLDF	VMC[a]	GFMC[a]
0.093	10.753	0.013 95	3.2	3.3	3.3
0.100	10.000	0.014 54	3.3		
0.120	8.333	0.016 05	3.7		
0.130	7.692	0.016 74	3.9		
0.150	6.667	0.017 95	4.2		
0.186	5.376	0.019 23	5.0	5.6	5.6
0.200	5.000	0.019 46	5.3		
0.300	3.333	0.020 92	7.5		
0.372	2.688	0.021 20	9.1	9.8	10.0
0.400	2.500	0.021 34	9.7		
0.500	2.000	0.021 58	12.0		
0.600	1.667	0.021 72	14.3		
0.650	1.538	0.021 73	15.5		
0.744	1.344			17.6	
1.116	0.896			25.6	
∞	0.000	0.021 84[b]			

[a] Values taken from Table I of [12].
[b] Value taken from Table II of [18].

the older value σ_∞(MC) $= 0.288 \pm 0.012$ K/Å^2. On the other hand, the ratio $\gamma_c/\gamma^0_{frf} = 0.67 \pm 0.10$ suggests a global retardation of the van der Waals force comparable to that found in [33] when analysing films adsorbed on solid substrates.

The fit of Skyrme-DF energy data to equation (4.3) with $a_5 = 0$ yielded $\gamma_c/\gamma^0_{frf} = 0.02 \pm 0.06$. The consistency with zero of this result can be attributed to the fact that this DF does not carry any information on the microscopic interaction between ^{4}He atoms, which tail originates the van der Waals force responsible for γ_c. A further manifestation of the lack of a finite-range two-body interaction may by observed in Figure 3, where the surface tension calculated with this DF approach attains the asymptotic value in a different way from that exhibited by data evaluated with NLDF formalisms containing the LJ potential. Having marked the particular characteristic of the Skyrme-DF, we can say that in the case of this zero-range functional the coefficients obtained from the fitting provide a good description of the behaviour of e as well as of σ_s. The latter quantity can be fairly well reproduced, as indicated by the dashed curve in Figure 3, by utilizing the expression

$$\sigma_s = \sigma_\infty + \frac{3}{2}\,\frac{\gamma_c}{n_c^2} + 2\,\frac{a_4}{n_c^3} + \frac{5}{2}\,\frac{a_5}{n_c^5}\,. \qquad (4.4)$$

The small difference between the results for σ_∞ and $\sigma_s^{expt} = 0.274 \pm 0.003$ K/Å^2 is due to the fact that, indeed, the parameter d_4 of the functional has been fixed in reference [18] by imposing this experimental value to a finite slab of helium rather than to the limiting case of the semi-infinite system.

Turning to the NLDF approaches, a glance at Table 2 indicates that in these cases the retardation of the van der Waals force amounts about $\gamma_c/\gamma^0_{frf} \simeq 0.3$, which is also of the order of the effect observed for films adsorbed on some surfaces [33]. Furthermore, Figure 3 shows that these formalisms provide reasonable predictions for the asymptotic value of the surface tension. In particular, the results σ_∞(OT-NLDF) are consistent with the experimental data of references [20,22]. It should be emphasized that in these NLDF theories the parameters of the functionals are determined without using values of σ_s^{expt}. The solid curve in Figure 3 indicates how well the OT-NLDF results for the surface tension are reproduced by the expansion of equation (4.4) when the coefficients extracted from the fit of the energy data are used. It should be also noticed that the present σ_∞(C-NLDF) agree with the value $\sigma_\infty = 0.287$ K/Å^2 obtained in reference [30] by fitting energy data of ^{4}He drops. On the other hand, it is worthwhile to mention that the results σ_∞(OP-NLDF) are a bit larger than the value $\sigma_s = 0.277$ K/Å^2 quoted in equation (28) of [24] because the latter quantity has been calculated for a finite system. The pointed curve in Figure 3 shows that the results for σ_1 obtained with the OT-NLDF are slightly larger than the MC estimates of the corresponding γ_1.

Let us briefly address to the stability question by looking at the incompressibility given by equation (3.25), which for thick species may be written in terms of γ_c and a_4

$$\frac{1}{n_c\,\kappa_s} \simeq 6\,\frac{\gamma_c}{n_c^3} + 12\,\frac{a_4}{n_c^4} = \frac{6\,\gamma_c}{n_c^3}\,\left(1 + \frac{2\,a_4}{\gamma_c}\,\frac{1}{n_c}\right). \qquad (4.5)$$

It can be readily verified that, upon replacing the pairs of values of γ_c and a_4 listed in Table 2 corresponding to each one of the NLDF approaches and to MC simulations, this expression always yields negative incompressibility over range of interest, *i.e.*, $n_c \geq 0.13$ Å^{-2}. This result confirms that thick free planar films are unstable in agreement with the conclusion drawn in [13,14].

In the following lines we shall examine the structure of the films. The reader may find a comparison between density profiles obtained from Skyrme-DF, OP-NLDF, and OT-NLDF calculations in Figure 4 of [31]. Therefore, we do not repeat here such a kind of drawing, but instead we directly focus the attention on the results for ρ_c, $z_{1/2}$, and W obtained with the DF approaches and the MC algorithms. Since the central density ρ_c and half-thickness $z_{1/2}$ provided by the different DFs are almost the same (see, *e.g.*, Fig. 4 in [31]), we only include in Table 3 the values calculated with the most recent proposal, *i.e.*, the OT-NLDF. The comparison of these ρ_c with those exhibited by the systems plotted in Figure 1 and 2 of [12] indicates a good quantitative agreement. The main feature of the central density is that for small systems it is significantly lower than the experimental equilibrium density of the bulk ^{4}He, $\rho_B^{expt} = \rho_0 = 0.02184$ Å^{-3}, while for increasing coverages it tends towards the saturation value. In addition, a glance at Table 3 indicates that the values of $z_{1/2}$ obtained with the OT-NLDF approach and the MC simulations are also in fair agreement.

We shall begin the analysis of W pointing out that the density profiles displayed in Figure 4 of [31] clearly indicate that the Skyrme-DF, the OP-NLDF, the C-NLDF, and the OT-NLDF approaches give different surface widths. From that graph one may conclude that the W obtained with the Skyrme-DF is noticeably larger than the other two. The present Figure 4 shows the behaviour of W over the whole range of examined coverages. From this plot one realizes that all the calculated widths with DFs are always larger than those obtained with MC techniques. For instance, at $n_c = 0.372$ Å^{-2} ($1/n_c = 2.69$ Å^2) the ratios of widths are W(GFMC)/W(Skyrme-DF) $= 0.56$, W(GFMC)/W(C-NLDF) $= 0.66$, W(GFMC)/W(C-NLDF) $= 0.68$ and W(GFMC)/W(OT-NLDF) $= 0.73$. By looking at the trend exhibited by the data displayed in Figure 4 one could conjecture that in the limit $1/n_c \to \infty$ all the sets of DF and MC widths would reach asymptotic values compatible with the measured width $W = 7.6^{+1}_{-2}$ Å reported by Lurio *et al.* [41]. The large size of the experimental error precludes to get any meaningful conclusion from the comparison of asymptotic values given by different DF approaches.

In summary, the relevant difference between the one-body densities obtained with DF approaches and MC methods appears at the fall out region of the film's density, where the profiles show larger gradients in the latter case. This feature suggests that systems calculated with

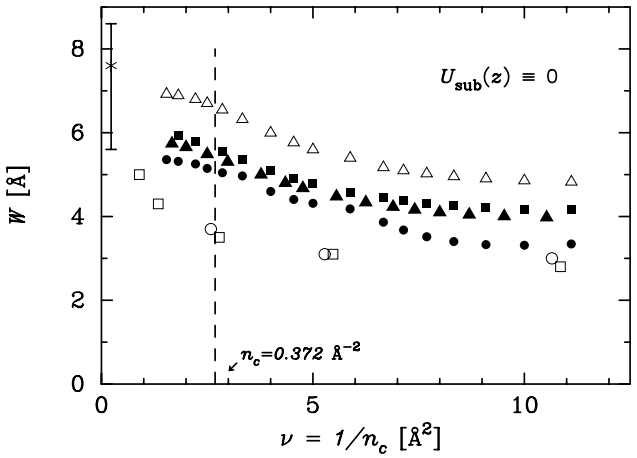

Fig. 4. Comparison of width W as a function of the inverse of coverage. Open squares and circles are VMC and GFMC data taken from Table I of reference [12]. The values of the Skyrme-DF are represented by open triangles. Full triangles, squares, and circles stand for results provided by the OP-, C-, and OT-NLDF approaches, respectively. The experimental value of reference [12] is indicated by a cross with the corresponding error bars. For visual purposes, the VMC and GFMC data evaluated at the same coverage are slightly got away from one another along the ν axis.

MC techniques are more rigid than those obtained within the NLDF theories. We suspect that this effect is due to the fact that DF and MC formalisms provide somewhat different correlations between particles in the low density region.

5 Final remarks

The fit of GFMC+VMC data to equation (4.3) yielded good results for the parameters of the adopted expansion for the correlation energy per particle. Perhaps, it would be interesting to carry out new MC simulations in order to decrease the statistical uncertainty of the energy values for diminishing their fluctuation and, in this way, to improve the χ^2/n_f of the adjustment. In addition, it would be useful to have MC data for coverages in the region $0.10 < n_c < 0.15$ Å^{-2}.

It is important to emphasize that, although the parameters of the DFs are determined for saturation conditions the energetics displayed in Figure 2 follows the trend of MC results until coverages at which the central density ρ_c is about one half of the equilibrium value ρ_0. In turn, Figure 3 shows that the bench of values of σ_∞ obtained within the frameworks of the examined NLDF approaches lies just above the set of experimental results. However, due to the fact that data of σ_s^{expt} were not used to fix the model parameters, the extracted surface tensions σ_∞ are good genuine predictions of these NLDF formalisms. In particular, σ_∞(OT-NLDF) agrees with the experimental values of references [20,22]. On the other hand, the quenching effect on γ_c is similar to the global retardation of the van der Waals force found in the analysis of adsorbed films in [33], except for the Skyrme-DF which does not contain any realistic information on the interaction between ^{4}He atoms. We may note in passing that all the examined NLDF approaches indicate that thick free films of ^{4}He are unstable in agreement with our previous studies [7,13,14].

The relevant discrepancy found in the present work is concerned to a structural characteristic of the films. Figure 4 shows that, for films with coverage ranging from $n_c \approx 0.15$ Å^{-2} up to $n_c \approx 0.60$ Å^{-2}, the thickness W of the ^{4}He-vacuum interface calculated with DFs is always larger than that obtained from MC simulations. The smallest difference corresponds to the most elaborated OT-NLDF, which reproduces better data of static response function and gives the best value of σ_∞. These results indicate that surfaces obtained with MC methods are more rigid than those yielded by DFs. This discrepancy suggests that the MC and DF theories provide somewhat different correlations between ^{4}He atoms at low density regimes. Therefore, it would be interesting to establish the extent to which this fact could produce sizeable effects when treating systems with markedly oscillating layered structure of the one-body density like films adsorbed onto strongly attractive substrates of graphite, Mg, H_2, etc. For instance, Figure 16 in [31] shows the very important difference between results for the velocity of third sound provided by the OP- and OT-NLDF.

Finally, we would like to stress that the detailed comparison performed in the present work among the results provided by different DF approaches and with the MC simulations is of current interest. This is due to the fact that DF formalisms are being nowadays widely utilized for studying inhomogeneous ^{4}He systems because the computational effort required by these calculations is feasible to be reasonably performed with the available facilities. For instance, the C-NLDF has been used in [42] to study instability scenarios for doped ^{4}He, a combination of OP-NLDF and OT-NLDF has been applied in [43] to examine the structure and energetics of mixed ^{4}He-^{3}He drops, and the OT-NLDF has been very recently utilized in [44] to investigate the structure and contact angle of liquid ^{4}He droplets adsorbed onto a Cs surface.

This work was supported in part by the Ministry of Culture and Education of Argentina through CONICET Contract PIP No. 4486/96 and under SIP Grant No. EX-01/TX55.

Appendix A: Hartree mean-field potentials

In this Appendix we shall give the explicit forms of the Hartree mean-field potentials $V_H(z)$ needed for the determination of the optimal local one-body density $\rho(z)$, because for the C- and OT-NLDF approaches they are not provided in the literature and in the case of the OP-NLDF one there is a misprint in equation (2.16) of the second paper of [11].

$$V_{\rm H}^{\rm OP}(z) = 4\,\pi\,\epsilon\,\sigma^2\,\left(\int_{-\infty}^{z-h} + \int_{z+h}^{\infty}\right) {\rm d}z'\,\rho(z')\left(\frac{\sigma}{z-z'}\right)^4\left[\frac{1}{5}\left(\frac{\sigma}{z-z'}\right)^6 - \frac{1}{2}\right] + 4\,\pi\,\epsilon\,\sigma^2\int_{z-h}^{z+h}{\rm d}z'\,\rho(z')\left(\frac{\sigma}{h}\right)^4$$
$$\times\left\{\left[\frac{8}{15}\left(\frac{\sigma}{h}\right)^6 - \frac{5}{6}\right] - \frac{1}{3}\left(\frac{z-z'}{h}\right)^6\left[\left(\frac{\sigma}{h}\right)^6 - 1\right]\right\} + \frac{c_4}{2}\,[\,\bar\rho(z)\,]^{\gamma_4+1} + \frac{3\,c_4}{8\,h}(\gamma_4+1)\int_{z-h}^{z+h}{\rm d}z'\,\rho(z')$$
$$\times\,[\,\bar\rho(z')\,]^{\gamma_4}\left[1 - \left(\frac{z-z'}{h}\right)^2\right], \qquad (A.7)$$

$$V_{\rm H}^{\rm OT}(z) = 4\,\pi\,\epsilon\,\sigma^2\,\left(\int_{-\infty}^{z-h} + \int_{z+h}^{\infty}\right) {\rm d}z'\,\rho(z')\left(\frac{\sigma}{z-z'}\right)^4\left[\frac{1}{5}\left(\frac{\sigma}{z-z'}\right)^6 - \frac{1}{2}\right] + 4\,\pi\,\epsilon\,\sigma^2\int_{z-h}^{z+h}{\rm d}z'\,\rho(z')\left(\frac{\sigma}{h}\right)^4\left[\frac{1}{5}\left(\frac{\sigma}{h}\right)^6 - \frac{1}{2}\right]$$
$$+\,\frac{c_4'}{2}\,[\,\bar\rho(z)\,]^2 + \frac{c_4''}{3}\,[\,\bar\rho(z)\,]^3 + \frac{3}{4\,h}\int_{z-h}^{z+h}{\rm d}z'\,\rho(z')\left[1 - \left(\frac{z-z'}{h}\right)^2\right]\left\{\,c_4'\,\bar\rho(z') + c_4''\,[\,\bar\rho(z')\,]^2\right\}$$
$$+\,\frac{\hbar^2}{2\,m}\,\frac{\alpha_{\rm s}}{\rho_{0s}}\int_{-\infty}^{\infty}{\rm d}z'\,F(\mid z-z'\mid)\left(\frac{{\rm d}\rho(z')}{{\rm d}z'}\right) I(z') + \frac{\hbar^2}{2\,m}\,\alpha_{\rm s}\,\frac{\rm d}{{\rm d}z}\left[\left(1 - \frac{\widetilde{\rho}(z)}{\rho_{0s}}\right) I(z)\right], \qquad (A.11)$$

For planar symmetry the correlation energy per particle in the case of the zero-range Skyrme DF is

$$e_{\rm c}^{\rm Sky}(z) = \frac{b_4}{2}\,\rho(z) + \frac{c_4}{2}\,\rho^{\gamma_4+1}(z) + d_4\,\frac{1}{\rho(z)}\left(\frac{{\rm d}\rho(z)}{{\rm d}z}\right)^2. \qquad (A.1)$$

The Hartree potential $V_{\rm H}^{\rm Sky}(\mathbf{z})$ derived by using the definition of equation (1.5) reads

$$V_{\rm H}^{\rm Sky}(z) = b_4\,\rho(z) + \frac{\gamma_4+2}{2}\,c_4\,\rho^{\gamma_4+1}(z) - 2\,d_4\,\frac{{\rm d}^2\rho(z)}{{\rm d}z^2}\,. \qquad (A.2)$$

In the case of the OP-NLDF approach the correlation energy per particle is

$$e_{\rm c}^{\rm OP}(z) = \pi\int_{-\infty}^{\infty}{\rm d}z'\,\rho(z')\int_0^{\infty}{\rm d}\eta\,\eta\,V_{\rm l}^{\rm OP}(R) + \frac{c_4}{2}\,[\,\bar\rho(z)\,]^{\gamma_4+1}, \qquad (A.3)$$

where R is the distance between two particles

$$R = \mid \mathbf{r} - \mathbf{r}'\mid = \sqrt{\eta^2 + (z-z')^2}, \qquad (A.4)$$

with η being the distance R projected onto the x-y plane

$$\eta = \mid \boldsymbol{\eta} - \boldsymbol{\eta}'\mid = \sqrt{(x-x')^2 + (y-y')^2}. \qquad (A.5)$$

In addition, the "coarse-grained density" $\bar\rho(z)$ is

$$\bar\rho(z) = \frac{3}{4\pi h^3}\int{\rm d}\mathbf{r}'\,\rho(z')\,\Theta(\,h - \mid \mathbf{r}-\mathbf{r}'\mid) = \frac{3}{4\,h}\int_{z-h}^{z+h}{\rm d}z'\,\rho(z')\left[1 - \left(\frac{z-z'}{h}\right)^2\right]. \qquad (A.6)$$

In turn, the self-consistent potential is, in agreement with equation (21) of [24],

see equation (A.7) above

with $h = h_{\rm OP}$.

In the C-NLDF proposal the correlation energy per particle is

$$e_{\rm c}^{\rm C}(z) = \pi\int_{-\infty}^{\infty}{\rm d}z'\,\rho(z')\int_0^{\infty}{\rm d}\eta\,\eta\,V_{\rm l}^{\rm C}\left(\sqrt{\eta^2 + (z-z')^2}\right) + \frac{c_4}{2}\,[\,\bar\rho(z)\,]^{\gamma_4+1}. \qquad (A.8)$$

The corresponding self-consistent potential is given by

$$V_{\rm H}^{\rm C}(z) = 4\,\pi\,\epsilon\,\sigma^2\,\left(\int_{-\infty}^{z-\sigma} + \int_{z+\sigma}^{\infty}\right){\rm d}z'\,\rho(z')\left(\frac{\sigma}{z-z'}\right)^4\left[\frac{1}{5}\left(\frac{\sigma}{z-z'}\right)^6 - \frac{1}{2}\right] - \frac{6}{5}\,\pi\,\epsilon\,\sigma^2\int_{z-\sigma}^{z+\sigma}{\rm d}z'\,\rho(z')$$
$$+\,\pi\,b_{\rm LJ}\,\sigma^2\int_{z-\sigma}^{z+\sigma}{\rm d}z'\,\rho(z')\left\{\left[1 - \left(\frac{z-z'}{\sigma}\right)^2\right] - \frac{1}{5}\left[1 - \left(\frac{z-z'}{\sigma}\right)^{10}\right]\right\}$$
$$+\,\frac{c_4}{2}\,[\,\bar\rho(z)\,]^{\gamma_4+1} + \frac{3\,c_4}{8\,h}(\gamma_4+1)\int_{z-h}^{z+h}{\rm d}z'\,\rho(z')\,[\,\bar\rho(z')\,]^{\gamma_4}\left[1 - \left(\frac{z-z'}{h}\right)^2\right], \qquad (A.9)$$

with $h = h_{\rm C} = h_{\rm OP}$.

Finally, within the framework of the OT-NLDF theory the correlation energy per particle is

$$e_{\rm c}^{\rm OT}(z) = \pi\int_{-\infty}^{\infty}{\rm d}z'\rho(z')\int_0^{\infty}{\rm d}\eta\,\eta V_{\rm l}^{\rm OT}\left(\sqrt{\eta^2 + (z-z')^2}\right) + \frac{c_4'}{2}\,[\,\bar\rho(z)\,]^2 + \frac{c_4''}{3}\,[\,\bar\rho(z)\,]^3. \qquad (A.10)$$

In turn, the Hartree potential reads

see equation (A.11) above

with $h = h_{\rm OT}$. Here $I(z)$ is the integral

$$I(z) = \int_{-\infty}^{\infty} \mathrm{d}z' \left(1 - \frac{\widetilde{\rho}(z')}{\rho_{0s}} \right) F(\mid z - z' \mid) \frac{\mathrm{d}\rho(z')}{\mathrm{d}z'}, \tag{A.12}$$

the weighted average density $\widetilde{\rho}(z)$ is

$$\begin{aligned} \widetilde{\rho}(z) &= \int d\mathbf{r}' \, \rho(z') \, F(\mid \mathbf{r} - \mathbf{r}' \mid) \\ &= \int_{-\infty}^{\infty} \mathrm{d}z' \, \rho(z') \, F(\mid z - z' \mid), \end{aligned} \tag{A.13}$$

and the weight $F(\mid z - z' \mid)$ is the one-dimensional function

$$F(\mid z - z' \mid) = \frac{1}{\sqrt{\pi}\,\ell} \, \mathrm{e}^{-(z-z')^2/\ell^2}. \tag{A.14}$$

References

1. *Proc. Inter. Symposium on Quantum Fluids and Solids Cornell University, Ithaca, New York, June 1995*, J. Low Temp. Phys. **101**, Nos. 1/4 (1995).
2. *Proc. Inter. Symposium on Quantum Fluids and Solids Paris, June 1997*, J. Low Temp. Phys. **110**, Nos. 1/2 (1998).
3. *Proc. Inter. Symposium on Quantum Fluids and Solids Amherst, Massachusetts, June 1998*, J. Low Temp. Phys. **113**, Nos. 3/6 (1998).
4. E. Cheng, M.W. Cole, J. Dupont-Roc, W.F. Saam, J. Treiner, Rev. Mod. Phys. **65**, 557 (1993).
5. E. Feenberg, *Theory of Quantum Fluids* (Academic, New York, 1969).
6. E. Krotscheck, G.-X. Qian, W. Kohn, Phys. Rev. B **31**, 4245 (1985).
7. L. Szybisz, M.L. Ristig, Phys. Rev. B **40**, 4391 (1989).
8. B.E. Clements, J.L. Epstein, E. Krotscheck, M. Saarela, Phys. Rev. B **48**, 7450 (1993).
9. B.E. Clements, H. Forbert, E. Krotscheck, M. Saarela, J. Low Temp. Phys. **95**, 849 (1994).
10. R.A. Aziz, V.P.S. Nain, J.S. Carley, W.L. Taylor, G.T. McConville, J. Chem. Phys. **70**, 4330 (1979).
11. E. Cheng, M.W. Cole, W.F. Saam, J. Treiner, Phys. Rev. Lett. **67**, 1007 (1991); Phys. Rev. B **46**, 13 967 (1992) [Erratum **47**, 14 661 (1993)].
12. J.L. Vallés, K.E. Schmidt, Phys. Rev. B **38**, 2879 (1988).
13. L. Szybisz, Phys. Rev. B **56**, 11 845 (1997).
14. L. Szybisz, Phys. Rev. B **58**, 109 (1998).
15. C. Carraro, M.W. Cole, Phys. Rev. B **46**, 10 947 (1992).
16. P. Hohenberg, W. Kohn, Phys. Rev. **136**, B 864 (1964).
17. W.F. Saam, C. Ebner, Phys. Rev. Lett. **34**, 253 (1975).
18. S. Stringari, J. Treiner, Phys. Rev. B **36**, 8369 (1987).
19. D. Vauterin, D.M. Brink, Phys. Lett. B **32**, 149 (1970); M. Beimer, H. Flocard, Nguyen Van Giai, P. Quentin, Nucl. Phys. A **238**, 29 (1975).
20. H.M. Guo, D.O. Edwards, R.E. Sarwinski, J.T. Tough, Phys. Rev. Lett. **27**, 1259 (1971); D.O. Edwards, W.F. Saam, in *Progress in Low Temperature Physics*, edited by D.F. Brewer (North-Holland, Amsterdam, 1978), Vol. 7A, Chap. 4.
21. M. Iino, M. Suzuki, A.J. Ikushima, J. Low Temp. Phys. **61**, 155 (1985); A.J. Ikushima, M. Iino, M. Suzuki, Can. J. Phys. **65**, 1505 (1987).
22. P. Roche, G. Deville, N.J. Appleyard, F.I.B. Williams, J. Low Temp. Phys. **106**, 565 (1997).
23. S. Stringari, J. Treiner, J. Chem. Phys. **87**, 5021 (1987).
24. J. Dupont-Roc, M. Himbert, N. Pavloff, J. Treiner, J. Low Temp. Phys. **81**, 31 (1990).
25. J. de Boer, A. Michels, Physica **6**, 945 (1938).
26. P. Tarazona, Phys. Rev. A **31**, 2672 (1985).
27. R.A. Cowley, A.D.B. Woods, Can. J. Phys. **49**, 177 (1971); A.D.B. Woods, R.A. Cowley, Rep. Prog. Phys. **36**, 1135 (1973).
28. M. Barranco, D.M. Jezek, E.S. Hernández, J. Navarro, Ll. Serra, Z. Phys. D **28**, 257 (1993).
29. D. Pines, Can. J. Phys. **65**, 1357 (1987).
30. M. Barranco, E.S. Hernández, Phys. Rev. B **49**, 12 078 (1994).
31. F. Dalfovo, A. Lastri, L. Pricaupenko, S. Stringari, J. Treiner, Phys. Rev. B **52**, 1193 (1995).
32. A. Lastri, F. Dalfovo, L. Pitaevskii, S. Stringari, J. Low Temp. Phys. **96**, 227 (1995).
33. L. Szybisz, J. Low Temp. Phys. **116**, 215 (1999).
34. C. Ebner, W.F. Saam, A.K. Sen, Phys. Rev. B **31**, 6134 (1985); *ibid.* **32**, 1558 (1985).
35. J.S. Rowlinson, B. Widom, *Molecular Theory of Capillarity* (Clarendon, Oxford, 1982).
36. E. Cheng, M.W. Cole, Phys. Rev. B **38**, 987 (1989) and references therein.
37. M. Wagner, D.M. Ceperley, J. Low Temp. Phys. **94**, 185 (1994).
38. W.L. McMillan, Phys. Rev. **138**, A 442 (1965).
39. K. Schmidt, M.H. Kalos, M.A. Lee, G.V. Chester, Phys. Rev. Lett. **45**, 573 (1980).
40. M.H. Kalos, M.A. Lee, P.A. Whitlock, G.V. Chester, Phys. Rev. B **24**, 115 (1981).
41. L.B. Lurio, T.A. Rabedeau, P.S. Pershan, I.F. Silvera, M. Deutsch, S.D. Kosowsky, B.M. Ocko, Phys. Rev. Lett. **68**, 2628 (1992); Phys. Rev. B **48**, 9644 (1993).
42. S.M. Gatica, E.S. Hernández, M. Barranco, J. Chem. Phys. **107**, 927 (1997).
43. M. Barranco, M. Pi, S.M. Gatica, E.S. Hernández, J. Navarro, Phys. Rev. B **56**, 8997 (1997).
44. F. Ancilotto, A.M. Sartori, F. Toigo, Phys. Rev. B **58**, 5085 (1998).